Quaternary Map, Active Faulting, Tectonic Geomorphology, and Uplift Rate of the Humboldt Range in the Basin and Range Province of Nevada, United States

Steven G. Wesnousky*[1]

ABSTRACT

Fault-truncated, uplifted, and abandoned alluvial fans are frequent along the western flank of the active normal fault bounded Humboldt range. Terrestrial cosmogenic nuclide surface exposure dating of a faulted terrace at Rocky Canyon indicates that uplift of the range has averaged about 0.12 mm/yr during the last ∼160 ka. A similar uplift rate of less than about 0.07 mm/yr over the last 35 ka or more years is estimated from offset of a younger terrace at the same site. Values of extension rate across the range are 0.04–0.07 mm/yr, if it is assumed that the range-bounding fault dips at 60°, in general accord with very low values of contemporary geodetic strain reported for the area. Geomorphology at Rocky Canyon records a period leading up to about 160 ka ago that erosion and aggradation of sediment along the rangefront were dominant over fault generated uplift, at which time faulting again became dominant, leading to uplift, incision, and preservation of ∼160-ka-old alluvial terraces here and elsewhere along the rangefront.

KEY POINTS

- The fault slip rate and tectonic geomorphology of a normal fault bounded Humboldt range are described.
- Repeated earthquakes are responsible for about 0.1 mm/yr of uplift during the last ∼160 ka.
- Observations add to understanding rates of fault slip and evolution across the Basin and Range.

Supplemental Material

INTRODUCTION

Peaks of the Humboldt range approach 3000 m in elevation adjacent to basins that rest at ∼1300 m. The range is bounded on its west flank by a normal fault, one of dozens that comprise the Basin and Range extensional province of the western United States (Fig. 1). The range-bounding fault is mapped to cut Holocene and Pleistocene alluvial deposits by Silberling and Wallace (1967) and Wallace *et al.* (1969). Wallace (1979) subsequently constructed 1:250,000 scale map of the entire trace and illustrated that the relative timing of past earthquakes and the relative rate at which faults slip is recorded in the morphology of fault scarps and normal fault-bounded rangefronts (Wallace, 1977, 1978). Silver *et al.* (2011) more recently utilized LiDAR to produce detailed contour maps, hillshade images, and fault trace maps along the central portion of the range. The range is exceptional in the abundance of landforms of varying age produced by earthquake displacements on the range-bounding fault. Efforts to construct maps of Quaternary deposits by relative age along the range though is limited to Davis (1983) mapping of the 7.5' Rye Patch quadrangle outboard of the main rangefront. Herein, I present a quaternary map of the rangefront, descriptions of range-bounding landforms formed by repeated uplift from earthquake displacements, and an estimate of the rate at which the range-bounding fault moves based on terrestrial cosmogenic nuclide (TCN) dating of uplifted deposits. The resulting observations are germane to geoscientists' efforts to quantify rates of fault slip, tectonic landform development, and extension across the Basin and Range.

1. Center for Neotectonic Studies and Nevada Seismological Laboratory, University of Nevada, Reno, Nevada, U.S.A., https://orcid.org/0000-0002-6734-6183 (SGW)

*Corresponding author: wesnousky@unr.edu

Cite this article as Wesnousky, S. G. (2023). Quaternary Map, Active Faulting, Tectonic Geomorphology, and Uplift Rate of the Humboldt Range in the Basin and Range Province of Nevada, United States, *Bull. Seismol. Soc. Am.* **XX**, 1–10, doi: 10.1785/0120220201

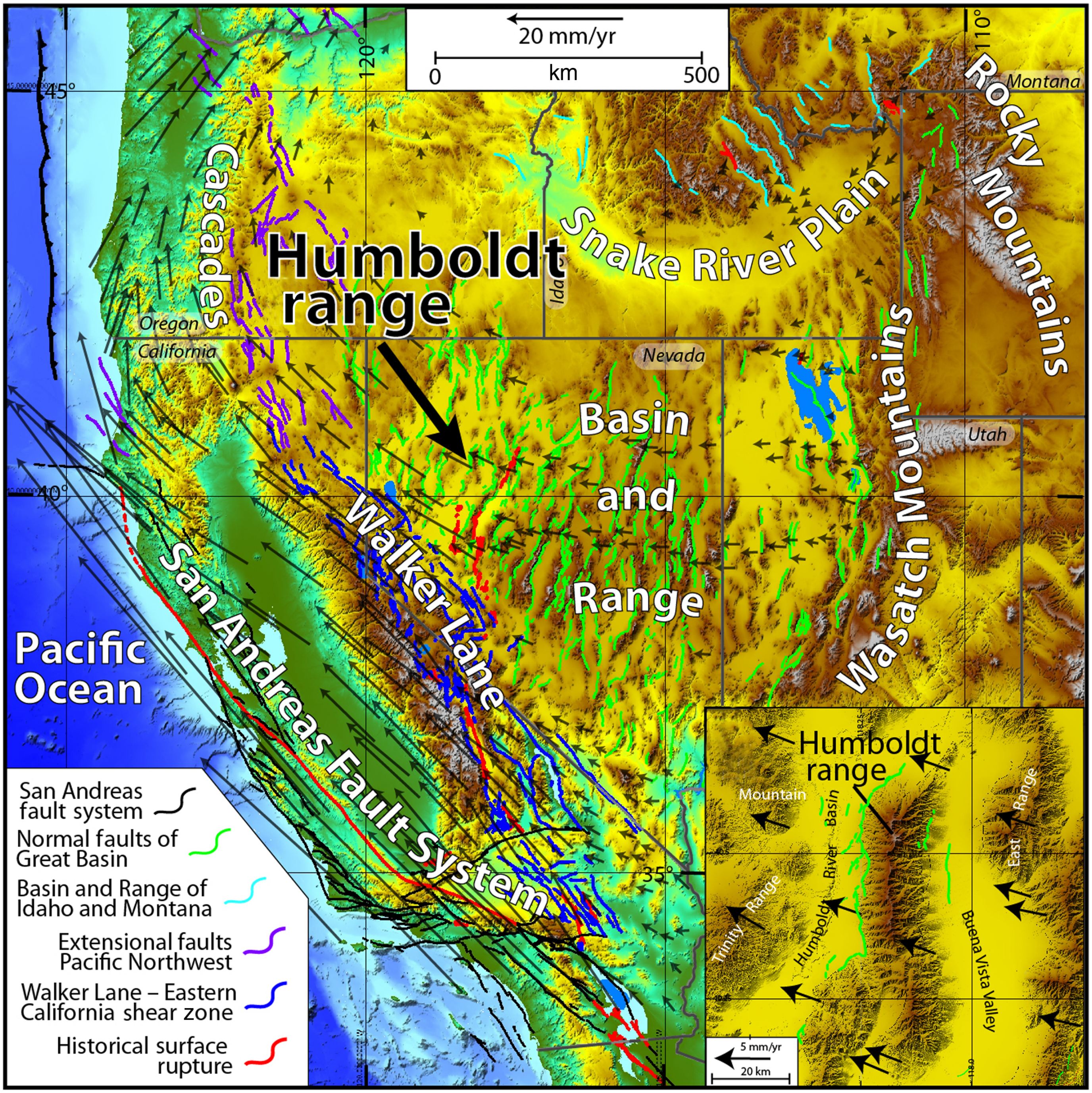

Figure 1. Location of Humboldt range on physiographic map displaying distribution of active faults and geodetic displacement vectors in western United States. Physiography from Becker *et al.* (2009), fault distribution modified from U.S. Geological Survey fault and fold database (USGS, 2020), and geodetic vectors plotted with respect to stable North American reference frame from (UNAVCO, 2020). (Inset) Shaded relief image of Humboldt and adjacent ranges plotted in context of denser distribution of geodetic vectors reported by Kreemer *et al.* (2012), also with respect to a stable North American reference frame. The color version of this figure is available only in the electronic edition.

REGIONAL TECTONICS

West directed extension across the basin and range is largely accommodated by displacement on active range-bounding normal faults (Fig. 1). Global Positioning System (GPS) measurements show east-directed extension of ~3 mm/yr is ongoing near and adjacent to the Wasatch Mountains. The extension is discernible by the abrupt increase of GPS vector lengths registered across the Wasatch Mountains. Moving west from the Wasatch, GPS vectors maintain a similar length and orientation across the central basin and range to about 117° W, indicating accumulation of extensional strain is minimal. Geodetic vectors begin to increase in length and progressively

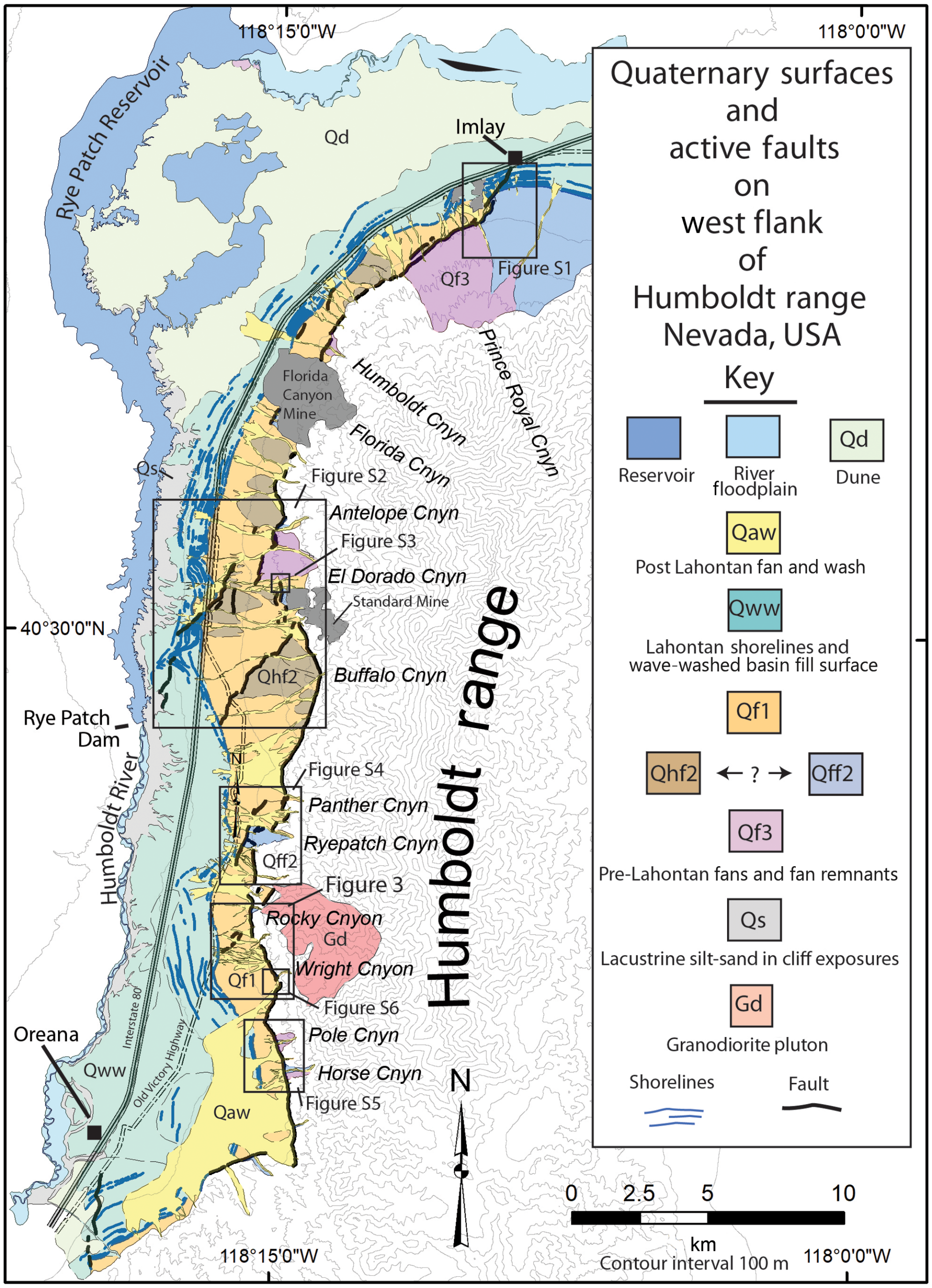

Figure 2. Map of Quaternary surfaces and site locations on west flank of Humboldt range. Location of map in Figure 3 is outlined by a box. Areal extent of additional maps (Figs. S1–S6) are also outlined by boxes and provided in the electronic supplement. The color version of this figure is available only in the electronic edition.

rotate northwestward to reflect right-lateral shear strain accumulation that characterizes the Walker Lane and San Andreas fault systems. The Humboldt range is in the area where displacement vectors begin to rotate northwestward. GPS displacement vectors across the Humboldt and adjacent ranges are not discernably different in length, indicating little if any ongoing strain accumulation (Fig. 1, inset). Analyses of the geodetic vector field limit strain accumulation to between 0 and 10^{-8}/yr (second invariant), equivalent to no more than ~0.3 mm/yr over a distance of 30 km (Kreemer *et al.*, 2012; Kreemer and Young, 2022).

MAPPING

The map of quaternary surfaces and active faults in Figure 2 is constructed from ≤~1:1000 scale topographic maps and hillshade images made from LiDAR, and photographs collected with an unmanned aerial vehicle (UAV). The collection, analysis, and preparation of imagery for the mapping follows that documented in numerous previous articles, among them Glennie *et al.* (2013), Johnson *et al.* (2014), and Angster *et al.* (2016). Black and white 1970 vintage 1:10 k low-sun angle aerial photography collected and kept in the Center for Neotectonic Studies further aided delineation of map units and fault traces.

Digital elevation models (DEMs) constructed from LiDAR data reported in Silver *et al.* (2011) are used for mapping along the central portion of the rangefront between about Buffalo and Humboldt canyons (west of 118° 12′ and north of 40° 28′). DEMs along the remainder of the rangefront are constructed from UAV imagery (~35,000 images). Spot spacing, and vertical and horizontal accuracies of the LiDAR DEM are reportedly 0.45, 0.15, and 0.45 m, respectively. DEMs constructed from UAV images are characterized by spot spacing of <0.25 m. Visual comparison of the DEMs constructed with the LiDAR and UAV imagery in regions where they overlap shows vertical accuracy of the DEMs constructed from the UAV imagery like that reported for the LiDAR.

Delineation of map units is based primarily on the degree of dissection and relative elevation of alluvial surfaces above modern stream grade. The approach has been applied and

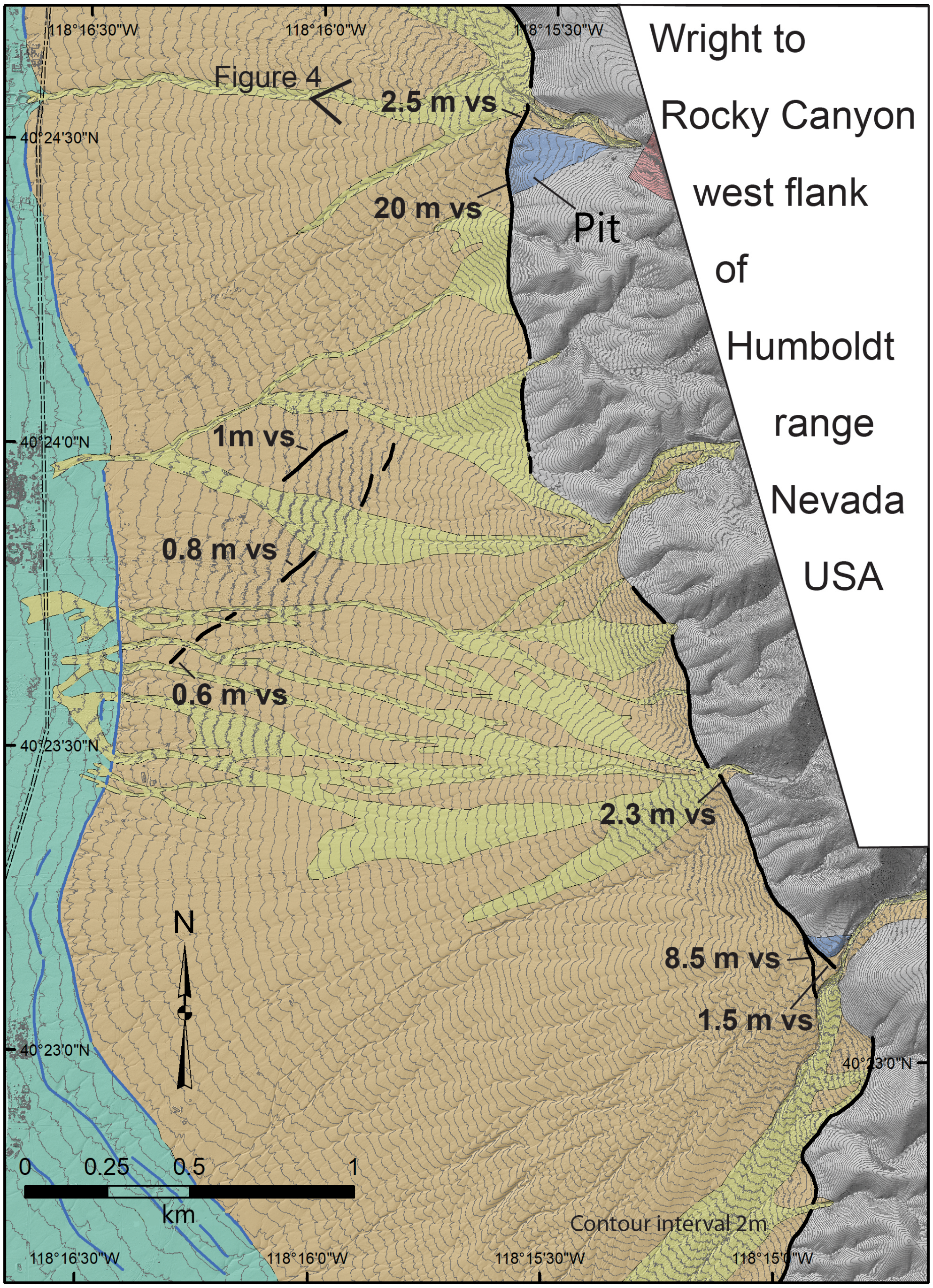

Figure 3. Map of Quaternary surfaces on 2 m contour base between Wright and Rocky canyons. Map units are the same as Figure 2 and vertical separation (vs) measurements annotated at points along fault traces. Location of pit used in this study for cosmogenic sampling and soil description. Open end of V symbol shows perspective of oblique photo in Figure 5. The color version of this figure is available only in the electronic edition.

documented previously (e.g., Dohrenwend, 1982a,b; Reheis *et al.*, 1995; Wesnousky, 2005). Unit Qww includes lacustrine surfaces and shoreline features preserved since the desiccation of pluvial Lake Lahontan that reached its highstand about 15,500 yr ago (Adams and Wesnousky, 1999; Briggs and Wesnousky, 2004). The youngest alluvial wash and fan deposits Qaw are those that cut or modify Qww deposits. Increasingly older alluvial fan and terrace surfaces are labeled Qf1, Qff2/Qhf2, and Qf3. Each is respectively higher than and cut by the active Qaw alluvial surface. Elements of Qf2 denoted Qff2 and Qhf2 are suspected to be similar in age. Situated on opposite sides of the main range-bounding fault and lacking any direct juxtaposition makes definitive correlation of the two units problematic. Dunes Qd and older lacustrine Qs deposits exposed in cliffs along the Humboldt River and Rye Patch Reservoir comprise the western limits of the map area. The granodiorite pluton (Gd) is the sole bedrock unit included because it is pertinent to analysis that follows. The map units and reason for delineating each are expanded upon in the supplemental material

RANGEFRONT MORPHOLOGY

The ~1:10,000 scale map and hillshade image respectively shown in Figures 3 and 4 are examples of mapping conducted along the range. The morphologic expression of the rangefront between Wright and Rocky canyons is generally representative of that observed along the length of the Humboldt rangefront: Rangefront faulting has produced an abrupt rangefront. Alluvial fan surfaces at the mouth of larger canyons have been truncated, uplifted, and abandoned by normal fault displacement along the rangefront; and shorelines of ~15,500-yr-old pluvial Lake Lahontan cut Qf1 and older fan elements emanating from the rangefront. Elsewhere fault splays departing from the rangefront are observed to cut Lake Lahontan shoreline features (e.g., Fig. 2). The oblique image at Rocky Canyon shown in

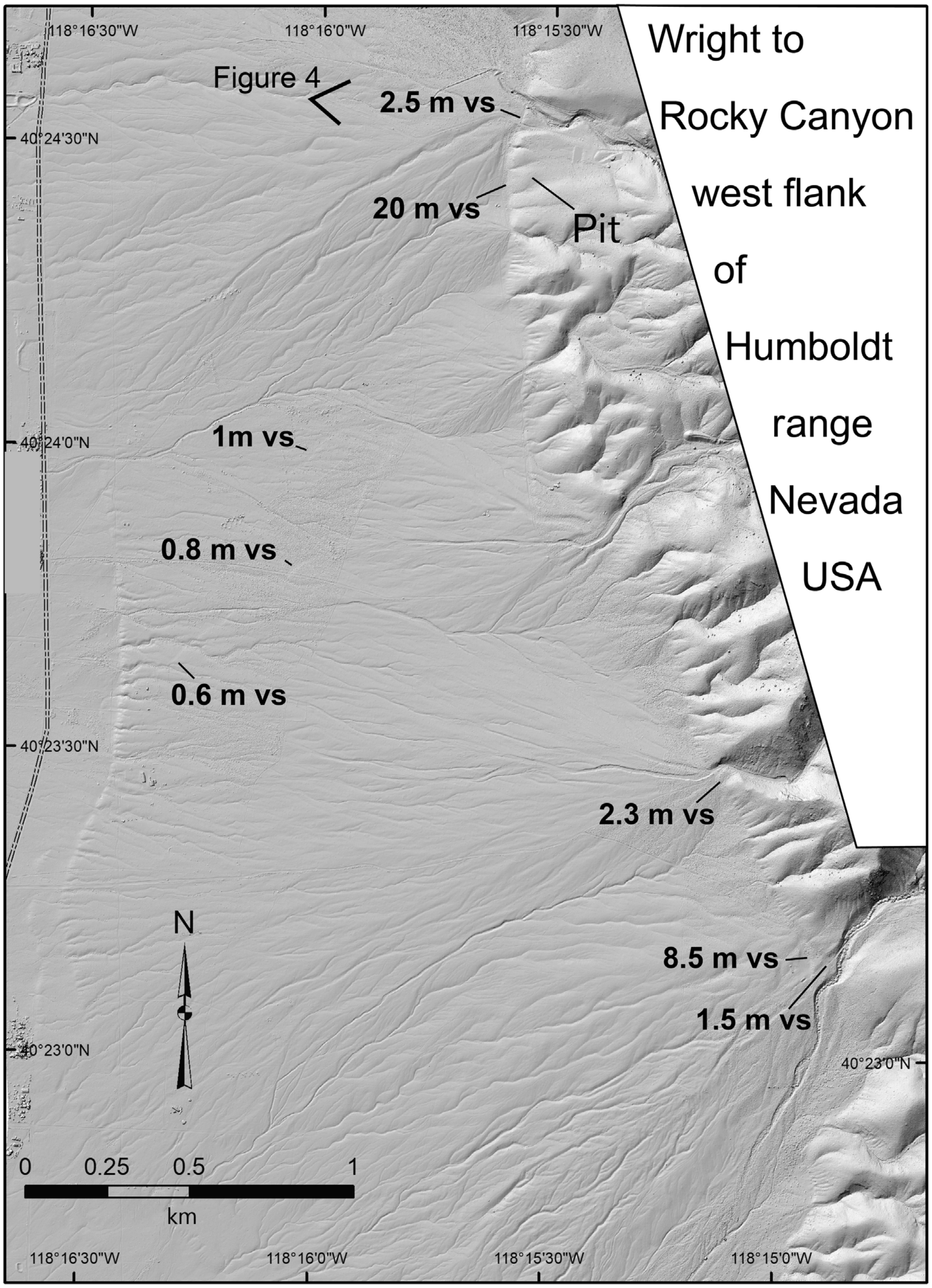

Figure 4. Hillshade image of map area in Figure 3.

AGE AND UPLIFT RATE OF ALLUVIAL SURFACES

The Qf1 and Qff2 surfaces at Rocky Canyon exhibit vertical separation (vs) of ~2.5 and 20 m, respectively (Figs. 3 and 4). The Qff2 scarp height is diminished where active fan alluviation originating at Rocky Canyon is burying the hanging wall (Fig. 5). Qff2 scarp heights are accordingly less near the mouth of the canyon and systematically increase away. The 20 m vs measure taken most distantly from the canyon mouth, where fan sedimentation of the hanging wall is absent or minimal, is the best measure of the tectonic offset of the surface.

An element of the Qf1 fan surface north of Rocky Canyon at El Dorado Canyon (Fig. 2; Fig. S3) is displaced by a fault scarp similar in size (2.7 m vs) to that observed at Rocky Canyon. Wesnousky *et al.* (2005) interpret the El Dorado Canyon scarp to have formed during two earthquakes during the last ~35 ka. The observation places the age of the Qf1 surface at ≥35 ka. A multi-displacement history of the Qf1 scarp at Rocky Canyon is also suggested by the steeper slope of the scarp near its base (oversteepening), though here the original morphology is disturbed by human excavations along the base (Fig. 5). Displacement of 2.5 m in ~35 ka equates to an average vertical uplift rate of ~0.07 mm/yr. The age reported by Wesnousky *et al.* (2005) for the offset surface is a minimum and associated with analytic uncertainties estimated at ±10 yr (Fig. S3). Discounting any small error in the measurement of displacement, the slip rate with the uncertainty is $\le 0.07^{+0.03}_{-0.02}$ mm/yr. Not knowing the number or timing of displacements over the time period of measurement adds additional uncertainty.

Figure 5 is illustrative of the greater fault offset of older as compared to younger alluvial surfaces that is commonly observed along the rangefront. Locations of additional maps and images displaying progressively greater offset of older alluvial surfaces and rangefront morphology at sites near Prince Royal, Buffalo, El Dorado, Panther, Horse, and Wrights canyons are marked by boxes labeled Figures S1–S6 in Figure 2 and archived as Figures S1–S6, available in the supplemental material to this article.

The Rocky Canyon drainage incises the sole granitic pluton along the rangefront (Fig. 2). The Qff2 fan surface for this

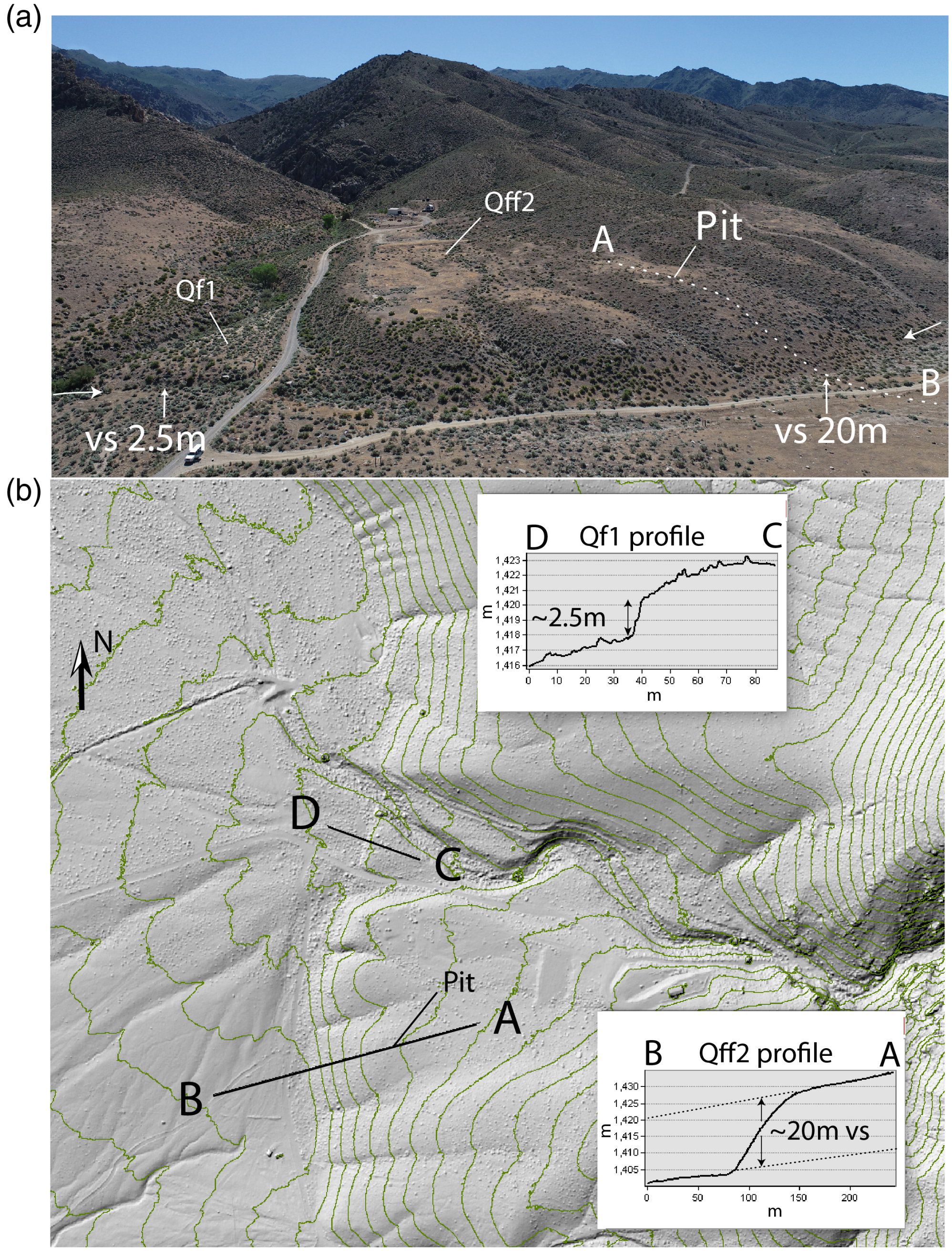

Figure 5. (a) Oblique view of fault-truncated alluvial surfaces at mouth of Rocky Canyon. Trace of fault extends along abrupt scarp between inwardly pointing arrows. Vs across Qff2 surface measured along profile marked by dotted line. Pit denotes location of soil description and sampling for terrestrial cosmogenic nuclide (TCN) surface exposure dating. The steepness of the lesser scarp bounding the Qf1 surface is accentuated by prior movements and scraping of earth by humans. (b) Digital elevation model with 5 m contours (green) constructed with unmanned aerial vehicle photography displaying location and elevation profiles across faulted surfaces at Rocky Canyon. Alluvial fan deposits are least near the fault on the hanging wall of Qff2 surface at cross-section AB, which records ∼20 m of vs. The slightly lesser slope on the hanging wall of AB profile may reflect sedimentation on the hanging wall or tectonic backtilting of the hanging wall that commonly occurs near the trace of normal faults. The color version of this figure is available only in the electronic edition.

reason contains considerable quartz and is amenable to TCN surface exposure dating using the ^{10}Be isotope (e.g., Gosse and Phillips, 2001). Quartz extraction and accelerator mass spectrometry (AMS) analysis for the 250 to 500 micron fractions of seven bulk samples taken at different depths within a pit located on the Qff2 surface (Fig. 5) are completed at Soil Characterization and Quaternary Pedology Lab of the Desert Research Institute, Nevada, and the PRIME Lab of Purdue University, respectively. Tables describing the Prime AMS measurements and measured ^{10}Be concentration for each sample are archived in Tables S1 and S2, and the latter plotted in Figure 6. The ^{10}Be concentration decreases smoothly as a function of sample depth. The concentration at any depth is a function of production rate of ^{10}Be, the decay rate of ^{10}Be, latitude, elevation, depth of sample below the surface, and density of material subject to cosmogenic radiation. The decay is a result of the progressively greater shielding from overburden such that cosmogenic radiation generally reaches no more than ∼2 m depth. The fitted curves are output of the Monte-Carlo simulator of Hidy *et al.* (2010), for which input and output files are placed in Tables S3 and S4. The modal value of acceptable curve fits corresponds to a TCN surface exposure age of 161^{+57}_{-29} ka, with maximum and minimum values encompassing the 2σ error. The vs across the surface at the pit is about 20 m. Dividing the value of vs 20 m by the surface exposure age indicates uplift of the Humboldt range has been $0.12^{+0.03}_{-0.03}$ mm/yr averaged over the last 161^{+57}_{-29} ka. The rate of extension assuming a 60° fault dip is half that.

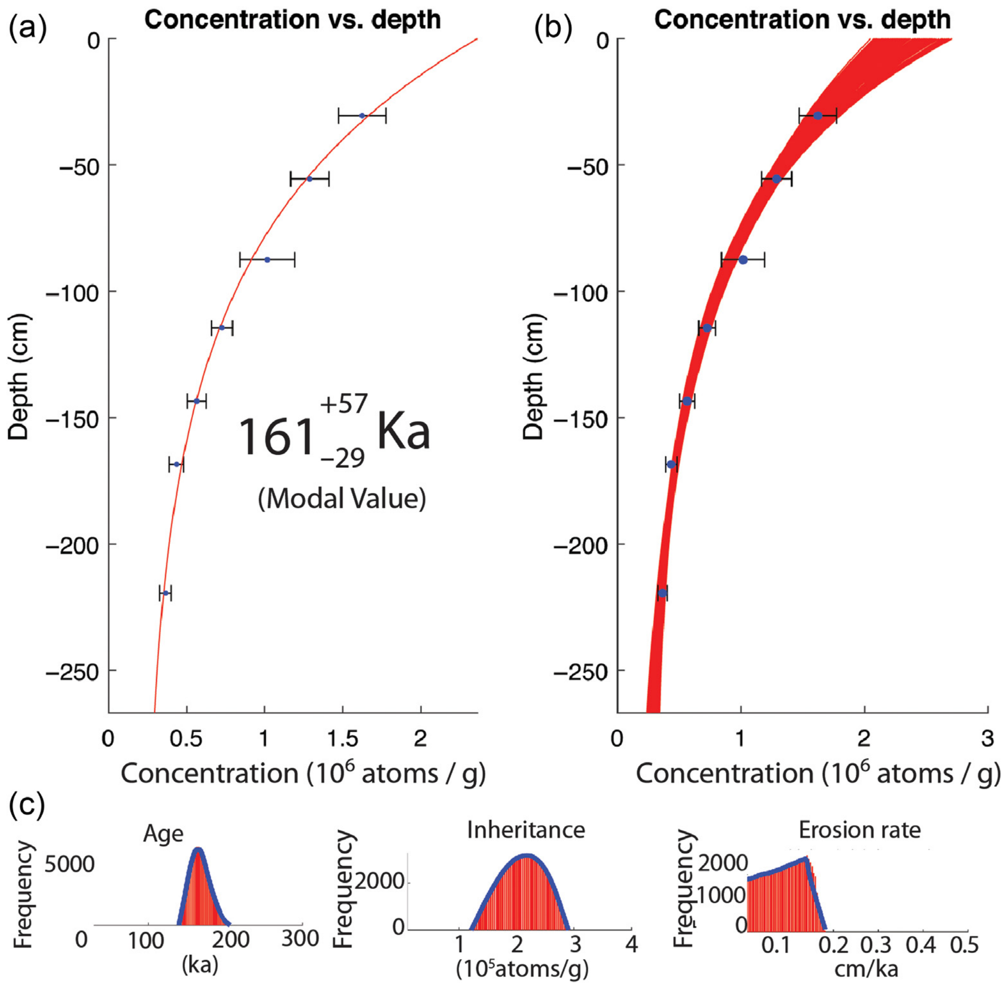

Figure 6. Depth profile of ^{10}Be concentration for samples collected in pit on Qff2 surface at Rocky Canyon (location in Figs. 3 and 4). Curve fits are calculated using the Monte Carlo approach and code of Hidy *et al.* (2010). The curve fits reflect the age of exposure, erosion of the Earth's surface, and contributions of ^{10}Be inherited from prior exposure of the sediment before deposition. (a) The best fitting and (b) range of acceptable curve fits. (c) Frequency distributions of values of age, inheritance, and erosion rate used in calculating acceptable curve fits. The modal value of age is 161 ka and the 2σ error of the distribution is reflected in the range of ages. Input files for analysis archived in the supplemental material. The color version of this figure is available only in the electronic edition.

SOIL DEVELOPMENT, AGE, AND ABANDONMENT OF ROCKY CANYON TERRACE

Description and textural analysis of the soil exposed in the same pit from which samples for TCN analysis were extracted exhibits a well-defined Bt layer of ~25 cm thickness underlain by a Bk horizon with carbonate development locally reaching stage IV (Fig. 7). The well-developed soil horizons give reason to interpret that the Qff2 surface at the location of the pit has not been subject to any significant erosion since abandonment of the surface on which it is developed. It is reasonably assumed that soil development commenced soon after the initial offset that began the abandonment of the Qff2 surface, much like it is commencing today on the adjacent and younger Qf1 surface (Fig. 5). The soil development observed in the pit may in turn be considered representative of what may be expected on similarly aged alluvial surfaces in surrounding regions of similar aridity.

The ~160 ka age of the uplifted and abandoned Qff2 surface at Rocky Canyon falls within and near the termination of stage VI of the oxygen-isotope record (Lisiecki and Raymo, 2005), a global period cooler temperatures. One may speculate that creation and abandonment of the Qff2 surface at Rocky Canyon (e.g., Fig. 5) and elsewhere along the range corresponds to relatively increased erosion and sedimentation across the rangefront during this time, and subsequent diminishment with global warming that occurred at the end of the stage VI. Addressing the speculation would require numerous studies like this be applied across the Basin and Range.

TECTONIC GEOMORPHOLOGY

The temporal development of the fault generated rangefront at Rocky Canyon is illustrated with sketches in Figure 8. The initial three sketches follow from the original study of Wallace (1978) showing the sequence of scarp development expected along an actively growing rangefront. The first depicts creation of a fault scarp on a smooth surface, followed in the next two by progressive uplift and erosion of the mountain front accompanying repeated earthquakes through time, finally resulting in an abrupt steep rangefront with triangular facets and ridges trending perpendicular to the rangefront. The subsequent panel 4 depicts a period in which deposition of debris from the eroding rangefront outpaces the rate of fault displacement, in effect broadening and filling the canyon with sediment. With cessation of deposition or an increasing rate of fault slip, or both, repeated fault offsets again truncate and uplift the rangefront, wherein sketch 5 stream incision cuts sediments on the footwall that are uplifted and leaves remnants as abandoned terraces. The abandoned terraces in this case

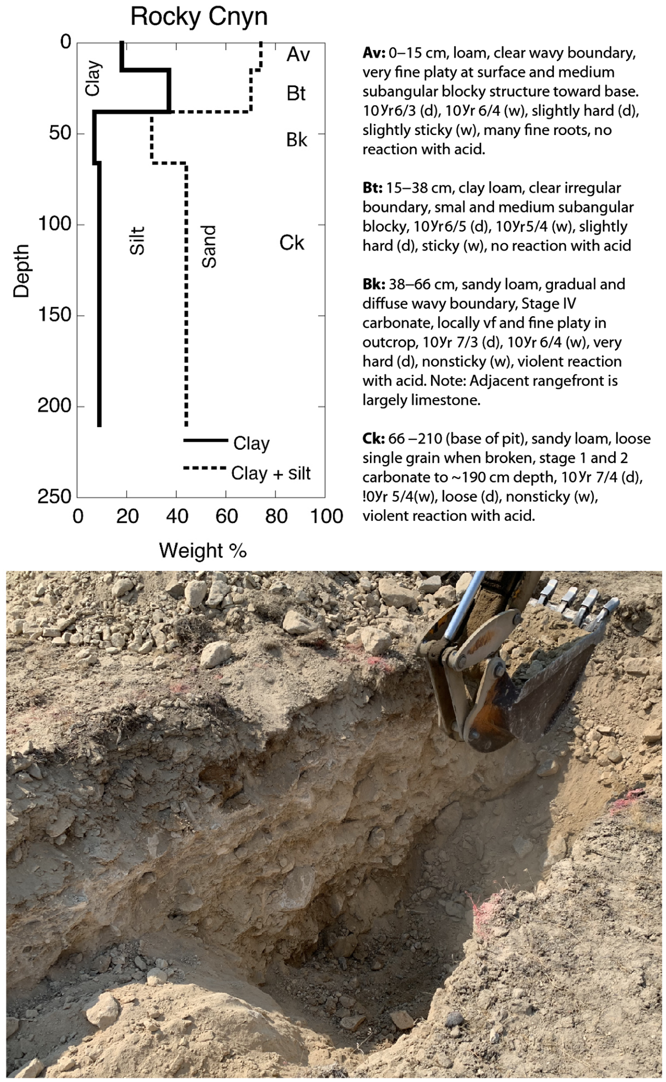

Figure 7. Soil texture profile and horizon descriptions above photo of pit on Rocky Canyon Qff2 surface. TCN depth profile of samples for this study extracted from same pit. Procedure of soil description follows practice outlined in Birkeland (1999) and Buol *et al.* (2011). The color version of this figure is available only in the electronic edition.

correspond to the Qff2 surface at Rocky Canyon. Finally, incision and broadening of the channel within the Qff2 surface continues until more recent earthquake offsets result in uplift and abandonment of a lower set of terraces, equivalent to the Qf1 surfaces at Rocky Canyon.

DISCUSSION AND CONCLUSION

The results are relevant to ongoing and future efforts to quantify rates of fault slip, landform development, and crustal extension across the Basin and Range. The majority of geologically assessed slip rates of range-bounding faults within the interior of the Basin and Range are derived from measured offsets of alluvial surfaces for which ages are qualitatively assessed from soil expression, and most often gauged to be no more than ~50–60 ka in age (Koehler and Wesnousky, 2011; Perouse and Wernicke, 2017). The viability of TCN surface exposure dating to quantitatively assess fault slip and mountain uplift rates over longer periods of time within the interior of the Basin and Range finds support in this study of Rocky Canyon. Further application of the method across the region holds the potential to better assess how slip rates have varied through space and time in the Basin and Range. Likewise, the coupled collection of TCN surface exposure ages and description of soils developed on those surfaces (e.g., Fig. 7) may ultimately serve to improve soil chronosequence observations currently used to evaluate the age of alluvial surfaces in the Basin and Range (e.g., see discussion in Koehler and Wesnousky, 2011).

Estimates of the vertical slip rates of two displaced alluvial surfaces at Rocky Canyon are $<0.07^{+0.03}_{-0.02}$ and $0.12^{+0.03}_{-0.03}$ mm/yr over the last $\geq 35^{+10}_{-10}$ and 161^{+57}_{-29} ka, respectively. The two values are indistinguishable in context of the uncertainties attendant to calculating the age of the offset surfaces, and not considered to be of sufficient resolution to conclude the rate has changed in any significant manner over the time period of measurement. The rates of crustal extension accompanying the uplift in the vicinity of 0.04–0.07 mm/yr if uplift of the alluvial surfaces is the result of displacement on an underlying fault dipping at 60°, as commonly assumed from frictional considerations for normal faults (Anderson, 1951). These low values of extension rate are also generally commensurate with the low values of contemporary strain accumulation recorded geodetically in the vicinity of the Humboldts (Fig. 1; Kreemer *et al.*, 2012).

DATA AND RESOURCES

The supplemental materials include expanded unit descriptions for maps of Figures 2 and 3, enlarged maps and oblique images of areas labeled Figures S1–S6 in Figure 2, and input and output data of terrestrial cosmogenic nuclide (TCN) surface exposure dating at Rocky Canyon are found in Tables S1–S4. Digital elevation models constructed from unmanned aerial vehicle (UAV) imagery collected in this study are archived at the Center for Neotectonic Studies, University of Nevada, Reno. Remaining data are from published sources listed in the References section.

DECLARATION OF COMPETING INTERESTS

The author acknowledges that there are no conflicts of interest recorded.

ACKNOWLEDGMENTS

Constructive comments from Zach Lifton, an anonymous reviewer, Peter Vikre, Joel Scheingross, Corné Kreemer, and editors Rich Briggs and Mark Stirling improved this article. Eli Silver provided access to LiDAR data along the central portion of the range. Sergei Matevosian graciously provided access to New Life USA property and excavations required for the cosmogenic analysis. Center for Neotectonic Studies Contribution number 86. Research supported by National Science Foundation Grant EAR 1920514.

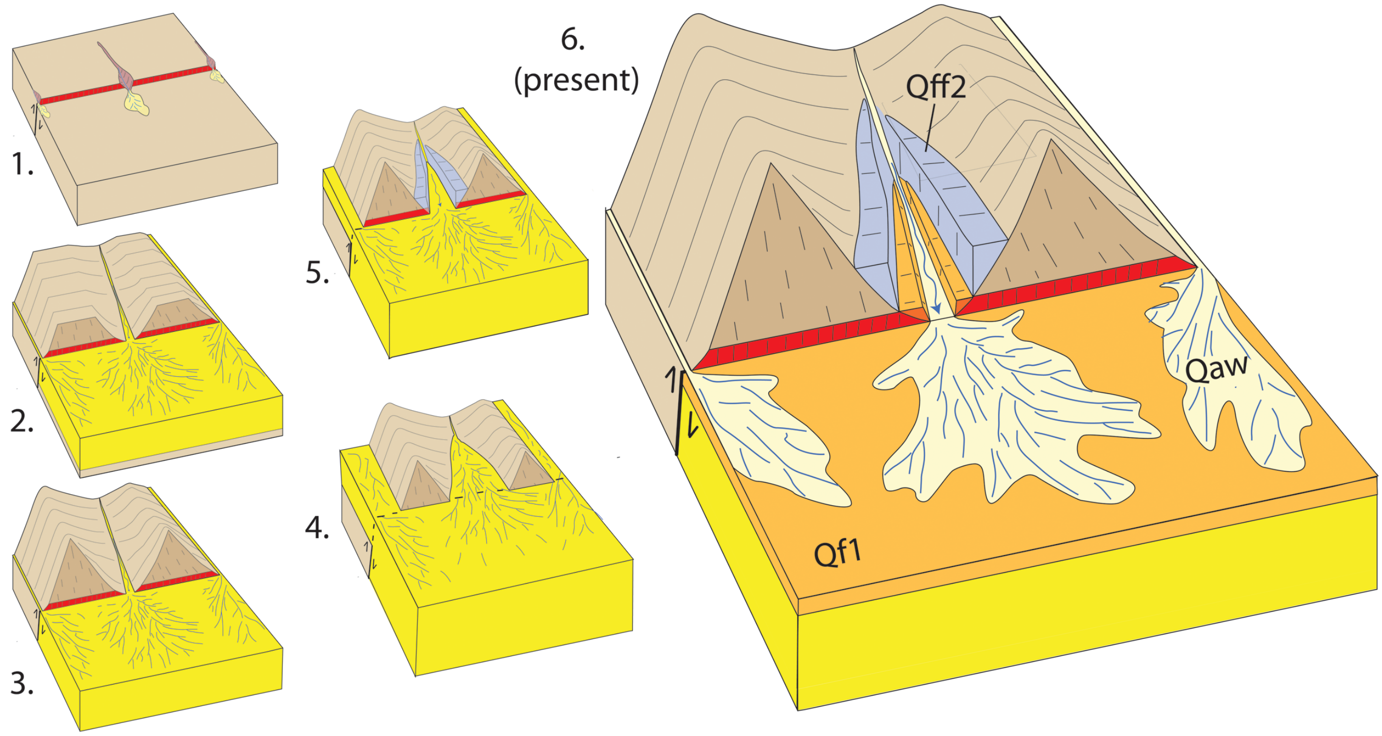

Figure 8. Sketches labeled 1–6 illustrating temporal development of range-front morphology from repeated normal fault displacements through time. The color version of this figure is available only in the electronic edition.

REFERENCES

Adams, K. D., and S. G. Wesnousky (1999). The Lake Lahontan highstand: Age, surficial characteristics, soil development, and regional shoreline correlation, *Geomorphology* **30,** 357–392.

Anderson, E. M. (1951). *The Dynamics of Faulting*, Oliver and Boyd, Edinburgh.

Angster, S., S. Wesnousky, W. L. Huang, G. Kent, T. Nakata, and H. Goto (2016). Application of UAV photography to refining the slip rate on the Pyramid Lake fault zone, Nevada, *Bull. Seismol. Soc. Am.* **106,** 785–798.

Becker, J. J., D. T. Sandwell, F. Smith, W. H. Braud, J. Binder, B. Depner, J. Fabre, D. Factor, J. Ingalls, S. Kim, *et al.* (2009). Global bathymetry and elevation data at 30 arc seconds resolution: SRTM30_PLUS, *Mar. Geod.* **32,** 355–371.

Birkeland, P. (1999). *Soils and Geomorhology*, Third Ed., Oxford University Press, Oxford, United Kingdom.

Briggs, R. W., and S. G. Wesnousky (2004). Late Pleistocene fault slip rate, earthquake recurrence, and recency of slip along the Pyramid Lake fault zone, northern Walker Lane, United States, *J. Geophys. Res.* **109,** doi: 10.1029/2003JB002717.

Buol, S. W., R. J. Southard, R. C. Graham, and P. A. McDaniel (2011). *Soil Genesis and Classification*, Wiley-Blackwell, Hoboken, New Jersey.

Davis, J. O. (1983). Geologic map of the Rye Patch Reservoir South quadrangle Nevada, *Nevada Bureau of Miners and Geology Map 76* (1:24k), 21 x 29 inch plate.

Dohrenwend, J. C. (1982a). Preliminary surficial geologic map of the Excelsior Mountains area, west-central Nevada, *U.S. Geol. Surv. Misc. Field Studies Map MF-1372*, 1:62,500, doi: 10.3133/mf1372.

Dohrenwend, J. C. (1982b). Reconnaissance surficial geologic map of the Gabbs-Luning area, west-central Nevada, *U.S. Geol. Surv. Misc. Field Studies Map MF-1374*, 1:62,300, doi: 10.3133/mf1372.

Glennie, C. L., W. E. Carter, R. L. Shrestha, and W. E. Dietrich (2013). Geodetic imaging with airborne LiDAR: The Earth's surface revealed, *Rep. Prog. Phys.* **76,** doi: 10.1088/0034-4885/76/8/086801.

Gosse, J. C., and F. M. Phillips (2001). Terrestrial in situ cosmogenic nuclides: Theory and application. *Quat. Sci. Rev.* **20,** 1475–1560.

Hidy, A. J., J. C. Gosse, J. L. Pederson, J. P. Mattern, and R. C. Finkel (2010). A geologically constrained Monte Carlo approach to modeling exposure ages from profiles of cosmogenic nuclides: An example from Lees Ferry, Arizona, *Geochem. Geophys. Geosys.* **11,** no. 9, doi: 10.1029/2010GC003084.

Johnson, K., E. Nissen, S. Saripalli, J. R. Arrowsmith, P. McGarey, K. Scharer, P. Williams, and K. Blisniuk (2014). Rapid mapping of ultrafine fault zone topography with structure from motion, *Geosphere* **10,** 969–986.

Koehler, R. D., and S. G. Wesnousky (2011). Late Pleistocene regional extension rate derived from earthquake geology of late Quaternary faults across the Great Basin, Nevada, between 38.5 degrees N and 40 degrees N latitude, *Geol. Soc. Am. Bull.* **123,** 631–650.

Kreemer, C., W. C. Hammond, G. Blewitt, A. A. Holland, and R. A. Bennett (2012). A geodetic strain rate model for the Pacific-North American plate boundary, western United States, *Nevada Bureau of Mines and Geology Map 178*, scale 1:1,500,000, plate: 48 × 46 inches.

Kreemer, C., and Z. Young (2022). Crustal strain rates in the western United States and their relationship with earthquake rates, *Seismol. Res. Lett.* **93,** 2990–3008.

Lisiecki, L. E., and M. E. Raymo (2005). A Pliocene-Pleistocene stack of 57 globally distributed benthic delta O-18 records, *Paleoceanography* **20,** doi: 10.1029/2004PA001071.

Perouse, E., and B. P. Wernicke (2017). Spatiotemporal evolution of fault slip rates in deforming continents: The case of the Great Basin region, northern Basin and Range province, *Geosphere* **13,** 112–135.

Reheis, M. C., J. Slate, and T. L. Sawyer (1995). Geologic map of late Cenozoic dceposits and faults in parts of the Mt. Barcroft, Piper Peak, and Soldier Pass 15' quadrangles, Esmeralda County, Nevada, and Mono County, California, *U.S. Geol. Surv. Misc. Investigations Series Map I-2464*, scale 1:24,000, doi: 10.3133/i2464.

Silberling, N. J., and R. E. Wallace (1967). Geologic map of the Imlay quadrangle: Pershing County, Nevada, *U.S. Geol. Surv. Map GQ-666* (1:62.500), doi: 10.3133/gq666.

Silver, E., R. MacKnight, E. Male, W. Pickles, P. Cocks, and A. Waibel (2011). LiDAR and hyperspectral analysis of mineral alteration and faulting on the west side of the Humboldt range, Nevada, *Geosphere* **7,** 1357–1368.

UNAVCO (2020). Tectonic motions of the western United States, *University NAVSTAR Consortium (UNAVCO) Velocity Map Poster Series*, available at https://www.unavco.org/education/resources//modules-and-activities/exploring-tectonic-motions/module-materials/map-western-us-motions-unavco-8.5x11.pdf (last accessed February 2023).

USGS (2020). United States Geological Survey Quaternary fault and fold database, available at https://earthquakes.usgs.gov/hazards/qfaults (last accessed June 2022).

Wallace, R. E. (1977). Profiles and ages of young fault scarps, north-central Nevada, *Geol. Soc. Am. Bull.* **88,** 1267–1281.

Wallace, R. E. (1978). Geometry and rates of change of fault-generated range fronts, north-central Nevada, *J. Res. U.S. Geol. Surv.* **6,** 637–649.

Wallace, R. E. (1979). Map of young fault scarps related to earthquakes in north central Nevada, *U.S. Geol. Surv. Open File Rept. 79-1554*, 1:125,000 map, doi: 10.3133/ofr791554.

Wallace, R. E., N. J. Silberling, W. P. Irwin, and D. B. Tatlock (1969). Geologic map of the Unionville Quadrangle: Pershing County, Nevada, *U.S. Geol. Surv. Map GQ-820* (1:62,500).

Wesnousky, S. G. (2005). Active faulting in the Walker Lane, *Tectonics* **24,** no. 3, doi: 10.1029/2004TC001645.

Wesnousky, S. G., A. D. Barron, R. W. Briggs, S. J. Caskey, S. Kumar, and L. Owen (2005). Paleoseismic transect across the northern Great Basin, *J. Geophys. Res.* **110,** doi: 10.1029/2004JB003283.

Manuscript received 8 October 2022